Correlation Length of Quasiperiodic Vortex Lattices

J. E. Villegas, M. I. Montero, C.-P. Li, and Ivan K. Schuller

Physics Department, University of California–San Diego, 9500 Gilman Drive, La Jolla, California 92093-0319, USA

(Received 20 February 2006; published 14 July 2006)

We investigated vortex-lattice dynamics in superconducting Nb thin films with different *quasiperiodic* arrays of magnetic pinning centers. The mixed-state magnetoresistance exhibits minima for well-defined applied fields, related to matching effects between the vortex lattice and those arrays. The results show that critical matching can originate at a local scale. For fractal arrays, the vortex-lattice correlation length is longer and the minima are deeper, close to those of periodic arrays.

DOI: 10.1103/PhysRevLett.97.027002 PACS numbers: 74.25.Qt, 47.32.C−, 74.78.Na

Vortex lattices (VLs) in type-II superconductors with periodic artificial pinning are useful for the study of the general problem of interacting ''particles'' moving in periodic potentials [1]. Among others, vortex dynamics has much in common with the dynamics of colloids [2], charge density waves [3], or Wigner crystals [4]. Commensurability between the VL and *periodic* pinning potentials leads to dramatic effects including enhanced pinning [5,6] and changes in the VL geometry [7]. Elasticity and correlation lengths are intimately related to these effects and are common ingredients to the general problem of commensurability.

Quasiperiodic (QP) potentials have received increasing attention since the discovery of quasicrystals [8]. Electrons [9] and atoms in QP potentials [10] have been investigated. A long-standing issue is whether commensurate states may exist on QP substrates [11]. Early experiments investigated flux quantization in quasicrystalline [12] and fractal [13] superconducting networks. Critical temperature oscillations as a function of applied field and recent numerical simulations of VL pinning by QP arrays [14] indicate some kind of ''commensurability.'' The latter would manifest as peaks in the field dependence of the critical depinning current.

Here we present an experimental study of the interaction between the VL and two different QP arrays of magnetic pinning centers: a 2D Fibonacci and a pentagonal self-similar fractal array. Comparison between both is interesting because of their different orientational order. Moreover, as opposed to the Fibonacci or Penrose arrays [14], the pentagonal array has fractal structure and exhibits ''periodic inflation'' symmetry: i.e., at any length scale (larger than the nearest neighbor distance), there is some portion which generates the whole array by repetition. Thus, the QP pentagonal array has some similarities also with periodic arrays.

We found minima in the mixed-state magnetoresistance that reveal matching effects between the VL and both QP potentials, reminiscent of those observed for periodic arrays, although they appear here in a *nonperiodic* series. Matching between the VL and the QP potential originates at a local scale for the Fibonacci array. The minima are deeper in the pentagonal than in the Fibonacci array, indicating that this fractal structure yields larger VL correlations.

Magnetic dot (Ni) arrays were prepared using a combination of e-beam lithography and sputtering [15]. Dots (40 nm height, $\varnothing = 280 \pm 10$ nm diameter) were covered by a 100 nm thick Nb thin film. This type of magnetic dots effectively pins superconducting vortices in Nb due to proximity effects and magnetic interactions [6]. A standard four-probe was defined by optical lithography and reactive ion etching, of total area $40 \times 40\ \mu\text{m}^2$. The superconducting critical temperature was $T_c = 7.50$ K ($T_c = 7.68$ K) for sample A (B). The mixed-state dc magnetoresistance was measured with the magnetic field B applied perpendicular to the film plane.

Sample A has a 2D Fibonacci array [Fig. 1(a)] constructed by applying iteratively the Fibonacci rule [14] to the line segments a and $a\tau$ [$a = 395$ nm and $\tau = (1 + \sqrt{5})/2 \approx 1.618$, the *golden ratio*], along the x and y axes. Thus, the distances between magnetic dots along these two directions follow the Fibonacci sequence $a, a\tau, a, a\tau, a\tau \ldots$, etc. The array of sample B [Fig. 1(c)] is generated from a pentagon of side a as the basic unit by performing an *inflation* operation: six pentagons [solid (blue) in Fig. 1(c)] arranged by locating five of them on the sides of the central sixth result in a scaled-up pentagon [hollow (red) in Fig. 1(c)]. To expand the array, the inflation operation is applied iteratively to the scaled-up pentagons. The sides of the pentagons grow as $a(1 + \tau)^\alpha$ and the sample contains a total of 6^α basic units (α is an integer, the ''order'' of the inflation). Note that pentagons are not space filling: For every six pentagons forming a scaled-up unit, five isosceles triangles fill the space left between the external ones.

The spectra of distances between dots were obtained using scanning electron microscopy. For sample A [Fig. 1(b)], some of the distances (black peaks) correspond to the basic lengths (a, $a\tau$) or their linear combinations $a(k + l\tau)$ (with k, l integers). Note that not all linear combinations are found in the Fibonacci array. The other

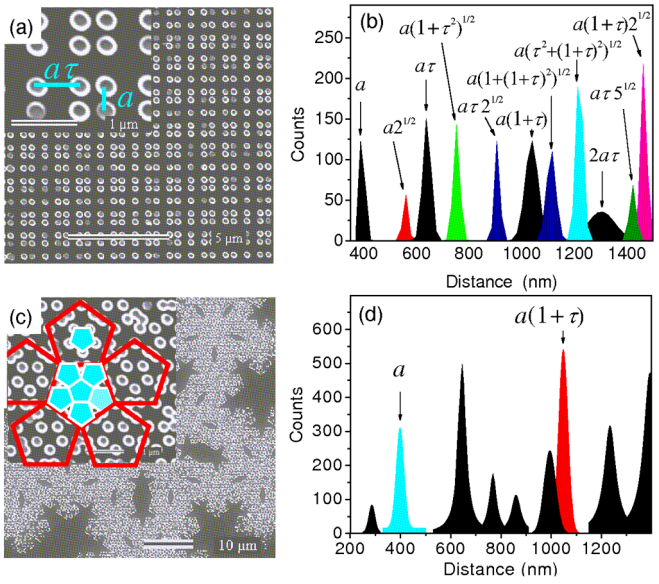

FIG. 1 (color online). (a) Electron microscopy images of sample A. (b) Spectrum of distances between dots for sample A. Peaks in black are for a, $a\tau$ and their linear combinations. The other peaks are for diagonals of the different rectangles in the array. (c) SEM image of sample B. A sketch of the construction of the array (see text) is shown with higher magnification. (d) Spectrum of distances between dots for sample B.

distances correspond to the diagonals of the different rectangles $a(k + l\tau) \times a(k' + l'\tau)$ found in the array. The area below each peak is proportional to the number of times that the corresponding rectangle is repeated in the array. The spectrum for sample B [Fig. 1(d)] contains, besides the distance corresponding to sides of the basic pentagons (a) and the first scaled-up one [$a(1 + \tau)$], many others [unlabeled in Fig. 1(d)] that are irrelevant in the present experiments.

The magnetoresistances of A and B are shown in Figs. 2(a) and 3(a) respectively. Both exhibit mixed-state magnetoresistance minima, implying enhanced VL pinning for well-defined applied fields (i.e., vortex densities). The common behavior of the two samples is (i) nonperiodic series of minima and (ii) the series of minima unrelated to the mean density of pinning sites in the array, but related to the mean densities of certain ''sublattices'' of the array. Besides the particular matching fields, the behavior of these two samples is different in two remarkable ways: symmetric (i.e., similar magnetoresistance for positive and negative fields) or strongly asymmetric background dissipation for the pentagonal (B) [inset in Fig. 3(a)] and the Fibonacci (A) array [Fig. 2(a)], respectively. Moreover, considerably deeper minima appear to higher fields for B, indicating stronger pinning.

Sample A exhibits a series of pronounced minima at the main matching fields (B_ν) for both positive and negative applied fields [solid vertical lines in Fig. 2(a) and its inset]. Some of the additional shallower minima are only observable for positive fields. The main minima correspond to the

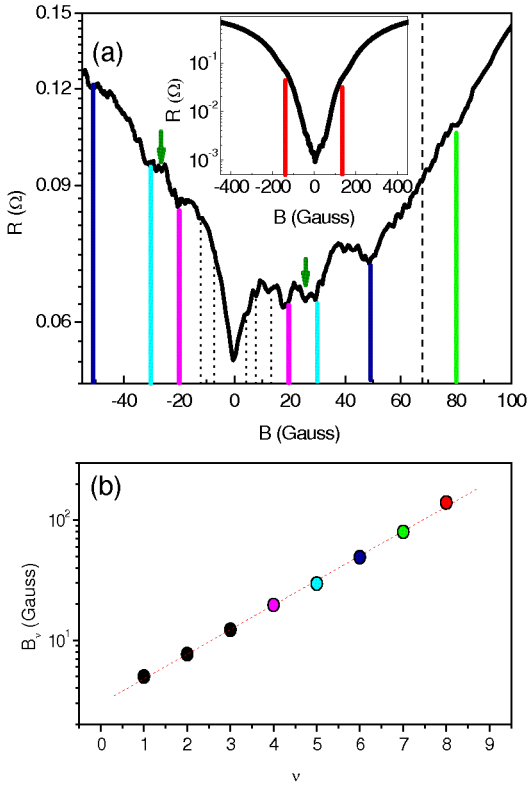

FIG. 2 (color online). (a) Magnetoresistance of sample A at $T = 0.989T_c$ and $J = 2.5\ \mathrm{kA\,cm^{-2}}$. Main minima are marked with vertical solid lines [the color code corresponds to that in Fig. 1(b)]. Minima marked with dotted black lines are within the Fibonacci series. The larger dashed black line indicates the matching field corresponding to the mean density of magnetic pinning sites. Inset: Magnetoresistance of sample A at $T = 0.988T_c$ and $J = 1.7\ \mathrm{kA\,cm^{-2}}$. (b) Main matching fields as a function of the order ν. Same color code as in (a). The solid line is the best fit to $B_\nu = B_0\tau^\nu$.

vortex density $d_v = B/\phi_0$ (B the applied field and $\phi_0 = 2.07 \times 10^{-15}$ Wb the flux quantum) being equal to $1/S$, where S is the area of the rectangles of the type $a(k + l\tau) \times a(k' + l'\tau)$. For instance, the minima at $B_\nu = \pm 80$ G correspond to the matching of the VL to the rectangles of area $S = a \times a\tau$ and $B_\nu = \pm 50$ G to the rectangles of areas $S = a\tau \times a\tau$ and $S = a \times a(1 + \tau)$. [The colors of the solid vertical lines in Fig. 2(a) correspond to the colors of the peaks in the spectra in Fig. 1(b) and identify the class of rectangles related to each matching field B_ν.] If the ratio of the basic lengths in this array is the golden ratio τ, the ratio of the areas of any two rectangles is $S/S' = \tau^\beta/q$ (with β and q integers). Therefore, the matching fields $B_\nu = \phi_0/S_i$ (S_i the area of rectangle i) belong to a Fibonacci series $B_\nu = B_0\tau^\nu/\mu$ (with ν and μ integers), in excellent agreement with the experimental data [Fig. 2(b)]. A logarithmic plot of the main matching fields as a function of order ν (with an arbitrary choice of the initial value of ν) yields $\log(B_\nu) = \log(B_0) + \nu \log(\tau_{\mathrm{exp}})$, with $\tau_{\mathrm{exp}} \approx 1.6$, very close to the golden ratio $\tau \approx 1.618$. Some of the shallower minima

[dotted black lines in Fig. 2(a)] are also contained in this Fibonacci sequence [black dots in Fig. 2(b)]. Other shallower minima correspond to subharmonics (i.e., $\mu > 1$) of the minima in the Fibonacci series. For instance, $B_\nu = \pm 25$ G [a subharmonic of $B_\nu = \pm 50$ G, arrows in Fig. 2(a)] correspond to matching to the rectangle $S = a\tau \times 2a\tau$. Finally, some other shallow minima could not be identified uniquely within our experimental resolution. These results are in good agreement with numerical simulations for 1D Fibonacci chains [14], where also a Fibonacci sequence of matching fields was found. The main difference is that here no minimum is found at the matching field corresponding to $d_{ps} = 3.2 \times 10^{12}$ m^{-2}, the mean pinning site density $B = d_{ps}\phi_0 \approx 66$ G [vertical dashed line in Fig. 2(a)]. Nevertheless, a calculation for a 2D Fibonacci array would be needed for better comparison with the experiment, since the in-plane anisotropy inherent to the 2D array may play an important role.

Sample B shows a series of deep ("main") minima and a number of much shallower ones between them [Fig. 3(a)]. A simple phenomenological model that mimics the experimental $R(B)$ uses the analytical expression

$$R(B) = R_b(B)\left(1 + A(B)\sum_{i=1}^{3} C_i \sin^2\left(\frac{B\pi}{B_{\phi i}}\right)\right). \qquad (1)$$

Here $R_b(B) = R_0 B$ (R_0 constant) describes the background dissipation expected in the Bardeen-Stephen limit [16]. The oscillations are simulated using three squared sinusoidal terms with different periods $B_{\phi i}$ and spectral weights C_i ($i = 1, 2, 3$). The term $A(B) = A_1 \exp(-B/A_2)$ (A_1, A_2 constants) accounts for the decreasing oscillation amplitude as field increases. The constants in Eq. (1) except the three periods $B_{\phi i}$ (five adjustable parameters) were chosen so that the simulated curve [inset in Fig. 3(b)] followed the general trends of the experimental one [Fig. 3(a)]. $B_{\phi i}$ reveal the physics in this model and were obtained taking into account the actual distribution of pinning sites. The most stable vortex distribution over the pentagons of side $a(1 + \tau)$ is assumed to be the one shown as an inset in Fig. 3(b). To calculate the corresponding matching field $B_{\phi 1}$, we considered the two types of "plaquettes" found in the array at this length scale: pentagons of side $a(1 + \tau)$ and triangles of equal sides and base $a(1 + \tau)(1 - \tau)$. Vortices on the vertices and sides of these plaquettes are shared by four and two of them, respectively, while vortices inside the pentagons are not shared. Thus, for this configuration the net number of vortices per pentagon (triangle) is $N_p = 8.75$ ($N_t = 1.75$). The corresponding matching field is given by $B_{\phi 1}(N_p, N_t) = \phi_0(n_p N_p + n_t N_t)/(n_p S_p + n_t S_t) = 96.7$ G, with S_p (S_t) the area of the pentagons (triangles) and n_p (n_t) the total number of pentagons (triangles) in the array. $B_{\phi 2}$ and $B_{\phi 3}$ correspond to the same vortex configuration shown in Fig. 3(b) (one vortex per vertex and side, plus five vortices inside the pentagon) over the self-similar pentagons of side $a(1 + \tau)^2$ and $a(1 + \tau)^3$, respectively. Thus, $B_\phi = B_{\phi 2}(1 + \tau)^2 = B_{\phi 3}(1 + \tau)^4$. Higher order terms were excluded (the size of larger scaled-up pentagons exceed the size of the array), as well as the term for the pentagon of side a (the corresponding matching field is of the order of B_{c2}). Since the ratios between $B_{\phi 1}$, $B_{\phi 2}$, and $B_{\phi 3}$ are irrational, these matching fields themselves do not appear in the resulting quasiperiodic series of minima, which reproduces with high fidelity the experimental one [Fig. 3(b)]. Most of the experimental minima are within ± 2 G of the calculated values. Only few minima in the theoretical (experimental) series are not found experimentally [(magenta) squares] and theoretically [(blue) triangles], respectively.

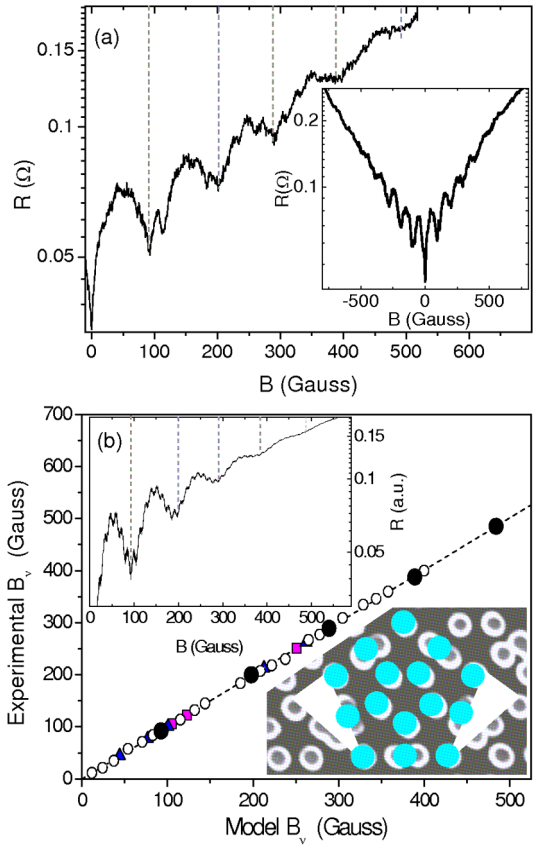

FIG. 3 (color online). (a) Magnetoresistance of sample B, at $T = 0.985T_c$ and $J = 1.5$ kA cm^{-2}. Vertical lines mark the main minima. Inset: Same curve as in (a) zoomed out. (b) Experimental matching fields (B_ν) vs theoretical ones [obtained with Eq. (1)]. Black dots are for the main minima, white ones for the shallower. Squares (magenta) are theoretical minima not found experimentally, triangles (blue) experimental minima not found theoretically. Inset: $R(B)$ simulated using Eq. (1) with $R_0 = 3 \times 10^{-4}$, $C_1 = 1$, $C_2 = 0.2$, $C_3 = 0.12$, $A_1 = 0.5$, $A_2 = 100$ G, $B_{\phi 1} = 96.7$, $B_{\phi 2} = 13.7$, and $B_{\phi 3} = 2$ G. Sketch: Distribution of vortices (cyan circles) at $B_\phi = 96.7$ G.

The results for the Fibonacci array indicate that critical matching between the VL and the array of magnetic dots originates at a local scale. The type of rectangles respon-

sible for a particular matching field are found scattered all over the array, leaving incommensurate spaces between them, and only cover a fraction of the array area (e.g., rectangles of area $S = a \times a$, $S = a \times a\tau$, and $S = a\tau \times a\tau$ cover 16%, 48%, and 36%, respectively). The VL matches the dot array wherever it finds one of these rectangles, while vortices between distribute to keep the mean vortex density. Thus, the VL is not regular all over the array. On the contrary, its geometry may change over nearest neighbor length scales, leading to a short VL correlation length close to a few hundreds of nanometers. This scenario is in agreement with experiments using both periodic and strong random pinning, which exhibit critical commensurability effects without long-range order of the VL [17]. Local matching yields shallow minima (resistivity changes below 5%) only at low magnetic fields [Fig. 2(a)] since matching is found repeatedly all over but not *everywhere* in the array. Vortices not located on magnetic pins move more easily. Moreover, the large elastic energy cost associated with irregular, nonperiodic distribution of vortices, is compensated by the gain in pinning energy coming from vortices in magnetic pinning. Since only a fraction of the vortices in the lattice are pinned by magnetic dots, the net pinning energy is small, leading to shallow minima, which do not appear at higher fields, where the elastic energy is too large and overcomes the pinning energy.

The situation is different for the pentagonal array. Here the magnetoresistance exhibits up to five main minima and a resistivity change of $\sim$35% for the first one. These values are closer to those of square arrays of same sized dots, with four main minima and a resistivity change of $\sim$60% for the first one [18]. Moreover, the pentagonal array exhibits self-similar matching over three different length scales, the larger of the order of several micrometers [$a(1 + \tau)^3 \approx 7\ \mu$m]. This implies VL correlation lengths around 1 order of magnitude larger than in the Fibonacci array. Since the entire array can be generated by repetition of the matching units (pentagons), here matching occurs everywhere over the array, as in periodic arrays. Thus, the net pinning energy after the cost of elastic energy is compensated is larger that in the Fibonacci array, yielding more pronounced minima up to higher fields.

As pointed out before, the background dissipation is strongly asymmetric for the Fibonacci array [see Fig. 2(a), field swept from positive to negative]. Since magnetic dots sizes are the same for both arrays (only the array geometry different), this effect is not connected to the magnetic state of the dots [19]. The asymmetry may be due to the more irregular distribution of pinning centers in the Fibonacci array. This implies that the time needed to establish a stable VL configuration is larger when new vortices enter the sample than when they exit (leaving pinned vortices behind), thus yielding stronger pinning when a field is reduced than when it is increased. Further experiments, including magnetization and magnetic relaxation, would be needed for better understanding of this behavior.

In summary, we found matching effects between the VL and different types of QP pinning potentials. The magnetoresistance shows quasiperiodic series of minima at well-defined applied fields. For the Fibonacci array, minima are shallower and appear at fields for which the VL matches the array of dots only on a local scale. This implies a short VL correlation length. On the contrary, for the pentagonal fractal array the minima are deeper and the series implies the occurrence of matching over longer length scales. This shows that the fractal structure of the pentagonal array preserves the long-range correlations of the VL.

This work was supported by U.S. NSF Grant No. DMR 03-53729. We acknowledge useful conversations and long time collaboration in related fields with Professor J. L. Vicent. J. E. V. thanks the Spanish MEC for financial support, Professor C. León for suggesting QP pinning, and J. Garcia-Barriocanal for an introduction to quasicrystals.

[1] T. Giamarchi and P. Le Doussal, Phys. Rev. Lett. **76**, 3408 (1996).
[2] P. T. Korda, M. B. Taylor, and D. G. Grier, Phys. Rev. Lett. **89**, 128301 (2002).
[3] G. Grüner, Rev. Mod. Phys. **60**, 1129 (1988).
[4] E. Y. Andrei *et al.*, Phys. Rev. Lett. **60**, 2765 (1988).
[5] O. Daldini *et al.*, Phys. Rev. Lett. **32**, 218 (1974); A. T. Fiory, A. F. Hebard, and S. Somekh, Appl. Phys. Lett. **32**, 73 (1978); A. Pruymboom *et al.*, Phys. Rev. Lett. **60**, 1430 (1988); Y. Otani *et al.*, J. Magn. Magn. Mater. **126**, 622 (1993); M. Baert *et al.*, Phys. Rev. Lett. **74**, 3269 (1995); J. I. Martín *et al.*, Phys. Rev. Lett. **79**, 1929 (1997); J. E. Villegas *et al.*, Science **302**, 1188 (2003).
[6] M. Montero, O. Stoll, and I. Schuller, Eur. Phys. J. B **40**, 459 (2004).
[7] J. I. Martín *et al.*, Phys. Rev. Lett. **83**, 1022 (1999).
[8] D. Shechtman *et al.*, Phys. Rev. Lett. **53**, 1951 (1984); D. Levine and P. J. Steinhardt, Phys. Rev. Lett. **53**, 2477 (1984).
[9] S. J. Poon, Adv. Phys. **41**, 303 (1992).
[10] L. Guidoni *et al.*, Phys. Rev. Lett. **79**, 3363 (1997).
[11] G. S. Grest, P. M. Chaikin, and D. Levine, Phys. Rev. Lett. **60**, 1162 (1988).
[12] A. Behrooz *et al.*, Phys. Rev. Lett. **57**, 368 (1986).
[13] J. M. Gordon *et al.*, Phys. Rev. Lett. **56**, 2280 (1986).
[14] V. Misko, S. Savel'ev, and F. Nori, Phys. Rev. Lett. **95**, 177007 (2005).
[15] J. I. Martín *et al.*, J. Magn. Magn. Mater. **256**, 449 (2003).
[16] J. Bardeen and M. J. Stephen, Phys. Rev. **140**, A1197 (1965).
[17] J. E. Villegas *et al.*, Phys. Rev. B **72**, 174512 (2005).
[18] A. Hoffmann, P. Prieto, and Ivan K. Schuller, Phys. Rev. B **61**, 6958 (2000).
[19] D. J. Morgan and J. B. Ketterson, Phys. Rev. Lett. **80**, 3614 (1998); M. J. Van Bael *et al.*, Phys. Rev. B **68**, 014509 (2003).